CERAMIC CROSS-FLOW MICROFILTRATION IN THE PRESENCE OF INSERTS

Petr MIKULASEK[1], Jiri CAKL[2] and Zbynek PETRAS

Department of Chemical Engineering, University of Pardubice, 532 10 Pardubice, Czech Republic; e-mail: [1] mikulase@hlb.upce.cz, [2] cakl@hlb.upce.cz

Received June 12, 1997
Accepted October 15, 1997

The influence of inserts with various configurations on permeate flux through a tubular ceramic microfiltration membrane was studied. The commercial metal-working oil emulsion was used in the experiments. A more extensive study of the effect of shear rate on permeate flux was made by comparing the steady-state flux of the empty tube system and the system with inserts. The cross-flow microfiltration with inserts was found to be simple and effective. Analysing experimental results, it was concluded that the introduction of inserts, irrespective of their configurations, resulted in a significant increase in permeate flux compared with results obtained in the empty tube system. The interruption of formation of a boundary layer by the inserts is attributed to mixing and migration of rejected particles from the membrane surface.

Key words: Microfiltration; Cross flow; Concentration polarisation; Membrane fouling; Inserts.

Cross-flow membrane microfiltration is a separation process for the removal of dispersed materials of sizes ranging from 0.05 to 10 μm from a liquid stream by forcing the liquid through a porous membrane. As opposed to dead-end microfiltration, where the dispersion is forced perpendicularly to the membrane, the dispersion in cross-flow filtration is forced tangentially to the membrane surface. It generates a number of forces which tend to remove the deposited layers from the membrane surface thus helping to keep the membrane relatively clean. The main applications of this process are found in the production of ultrapure water, food processing and dairy products, recovery of electrodeposition paints, treatment of oil and latex emulsions, and in biotechnology oriented applications such as fractionation of fermentation broths and high performance reactors for enzymatic and fermentation processes.

However, the present cross-flow membrane processes for liquid feed streams are still complicated by the phenomena of membrane fouling and of concentration polarisation in the liquid boundary layer adjacent to the membrane wall. Concentration polarisation and membrane fouling are major concerns in the successful use of a membrane-based separation operation as their net effect is to reduce the permeate flux thereby resulting in loss of productivity. Therefore, there is a tremendous potential to reduce or control concentration polarisation and fouling in membrane processes and hence alleviate these

limitations. The flux decline due to membrane fouling is frequently masked by changes in membrane properties or the feed solution or the development of concentration polarisation. The concentration polarisation results in a localised increase in the solute concentration on or near the membrane surface. This solute build-up lowers the flux due to an increase in hydrodynamic resistance in the mass boundary layer and due to an increase in local osmotic pressure resulting in a decreased net driving force. However, the concentration polarisation effects are reversible since they can be reduced by decreasing the transmembrane pressure or lowering the feed concentration. Fouling effects, on the other hand, are usually characterised by an irreversible decline of the flux. Although neither concentration polarisation nor membrane fouling can generally be avoided in membrane separations there are several possible approaches to reduce or control their extent.

Many different approaches can be chosen to improve the flux in these systems. The basic methods involve: changes in surface characteristics of the membrane, pre-treatment of the feed, and fluid management methods[1,2]. The feed flow management (hydrodynamic) approach to improving the flux consists either in the reduction of concentration polarisation by increasing the mass transfer away from the membrane or in the reduction of fouling based on increasing the wall shear rate and/or scouring the membrane surface.

Various shapes of static turbulence promoters such as static rods[3], spiral wire[4], metal grills[5], disc and doughnut shape inserts[6], Kenics proprietary static mixers[7,8], conical inserts[9] and recently reported helical baffles[10] have been used in ultrafiltration and microfiltration of various fluids with or without superimposing pulsating flow. In most cases, experimental results with inserts have been obtained using polymeric membranes, and, in the case of tubular membranes, the inner diameters were more than 10 mm.

This paper shows the effects of various static rods and the Kenics static mixer on the performance of a cross-flow microfiltration system with a tubular ceramic membrane. Here we present experimental results obtained in a device containing the turbulence promoters placed centrally. The irregular flow of the feed around both the membrane surface and the inserts can be responsible for the improved permeate flux and thereby to reduce the resistance of the boundary layer near the membrane surface.

EXPERIMENTAL

Membranes

The ceramic membranes used in this work were asymmetric, three-layered alumina membranes (Teronic, Czech Republic). They were configured as single cylindrical tubes 200 mm long, 6 mm ID and 10 mm OD (inner membrane area of 37.7 cm^2) consisting of a thin α-alumina layer deposited on the internal surface of the tubular alumina support. In our experiments, the microfiltration membranes

were used with the mean pore diameter equal to 0.1 μm. The pore size distribution of the membrane used (Fig. 1) was determined by the liquid displacement method[11].

Feeds

The commercial metal-working oil emulsion ERO-SB (Paramo, Pardubice, Czech Republic) was used in cross-flow microfiltration experiments. The 0.5 mass % emulsion was stable during the experiments. The size distribution of the oil drops in the emulsion used, shown in Fig. 1, was determined by a particle sizer BI-90 (Brookhaven Instruments Corp.).

Equipment

The microfiltration studies were carried out in a membrane filtration unit equipped with ceramic membranes. The fluids were circulated through the module by a centrifugal pump from the bottom of the storage tank under pressure into the membrane filter while both the concentrated dispersion and the permeate were recirculated back into the retentate container. Therefore, the concentration in the

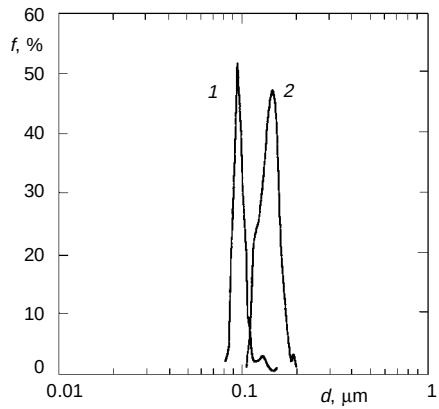

FIG. 1
Pore size distribution of 0.1 μm membrane (*1*) and drop size distribution of oil emulsion used (*2*)

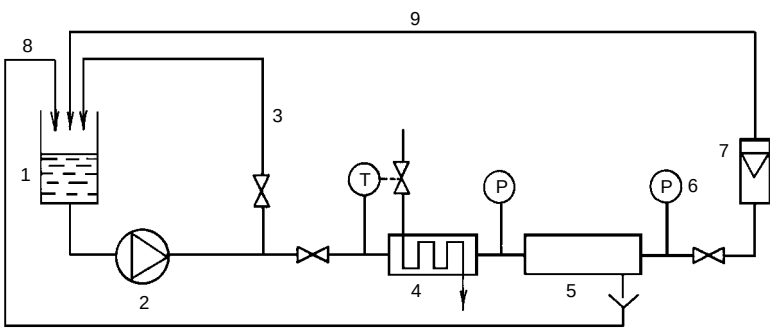

FIG. 2
Scheme of experimental apparatus: 1 storage tank; 2 pump; 3 by-pass; 4 thermal regulating system; 5 microfiltration module; 6 pressure gauges; 7 flow gauge; 8 permeate stream; 9 retentate stream

storage tank remains virtually constant. The unit made it possible the studies in which the transmembrane pressure and the cross-flow velocity were independently varied by the regulation system.

A schematic diagram of the experimental apparatus is shown in Fig. 2. It consisted mainly of a storage tank 1, a pump 2, a microfiltration module 5, equipped with a thermal regulation system 4, and a pressure 6 and a flow 7 control system.

At first, the flow of oil emulsion through the membrane was examined under various transmembrane pressures in the range 0–250 kPa while the superficial velocity was fixed at a constant value. Then the oil emulsion was measured at a constant transmembrane pressure ΔP = 200 kPa. For various superficial velocities in the range 0.15–3.1 m s^{-1}, the permeate flux, J, was evaluated. A new membrane was used in each set of experiments. Before and after the run, the pure water flux through the membrane was measured under the same conditions until the steady state was obtained. The differences in the steady-state pure water flux were taken as a measure of the fouling tendency of the membrane. The permeate mass and the filtration pressure data were synchronised by use of a balance interfaced with a computer. Therefore, simultaneous measurements of the cumulative permeate mass and the pressure were obtained. Every experiment was carried out until the flux became actually constant (± 2 l m^{-2} h^{-1}).

Solid metal rods (stainless steel) of different outer diameters (2, 3, 4, 5 mm) and Kenics static mixer as turbulence promoter were used. These inserts were centrally supported inside the membrane by the help of cross–shaped supports placed in the housing of the membrane. The rod inserts provided an annular space between the rod and the membrane inner surface. The Kenics static mixer, which is a twisted tape insert with alternating right- and left-hand pitch, consisting of 18 elements of stainless steel was used. The diameter of the mixer was smaller than that of the tubular membrane, leaving a small clearance between the outer edges of the elements and the membrane surface. The length of the element was equal to its diameter.

RESULTS AND DISCUSSION

Experimental results were obtained using various modes of membrane module configurations, such as an empty tubular membrane (ET), a membrane with a rod insert (RI), and a membrane with a Kenics static mixer (KM).

Effect of Transmembrane Pressure Difference on Flux

In Fig. 3, the typical steady-state flux data for different superficial velocities are plotted *versus* the transmembrane pressure difference. It was found that the flux increased with the pressure difference at low values up to a critical pressure difference, then the rate of increase decreased, and finally the flux became nearly independent of the pressure difference at high values. Thus, the well-known limiting flux behaviour[2,12] is observed which suggests that there is little advantage to be gained from the operation at higher pressure differences than 200 kPa. On the other hand, these findings indicate that the membrane resistance is dominant for low transmembrane pressure differences whereas the boundary layer control is dominant for higher ones. Since the control of boundary layer by proper inserts in membrane module is the point of this study, all the consequent experiments were carried out at the transmembrane pressure difference of 200 kPa.

Effect of Reynolds Number on Flux

The Reynolds numbers were calculated by the following relation

$$Re = u D_e \rho/\mu \ , \qquad (1)$$

where D_e is the equivalent hydraulic diameter.

For all modes, D_e is calculated as

$$D_e = 4 S/o \ , \qquad (2)$$

where S is the cross-sectional area available for flow and o is the wetted perimeter of the channel.

The steady-state permeate flux, J_{SS}, through the membrane as a function of the Reynolds number using different inserts is shown in Fig. 4. As expected, the values of steady-state fluxes for RI and KM modes are higher than those obtained in ET mode for the same value of Reynolds number. No transition is visible between turbulent and laminar flow around Re = 2 300, an effect attributable most probably to the lateral flow of the fluid through the porous membrane, thus preventing the onset of turbulence. The transition is expected to be observed at a much higher Reynolds number. Generally, the behaviour of the fluid flow in a porous channel is different from that in a nonporous-wall channel. In case of cross-flow microfiltration, the flow may be close to the transition between laminar and turbulent when the Reynolds number changes from 2 300 to nearly 6 000 depending on the module geometry, superficial velocity and permeate flux through the membrane[13].

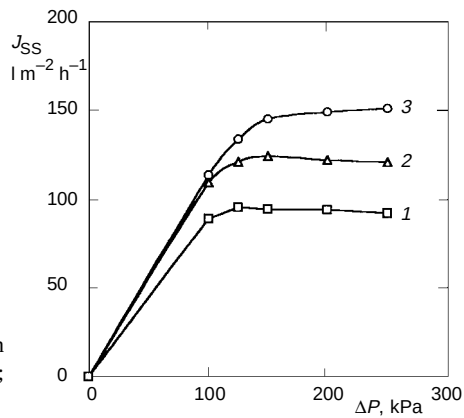

FIG. 3
Effect of transmembrane pressure difference on steady-state flux for the ET mode: *1* u = 1.49 m s^{-1}; *2* u = 1.98 m s^{-1}; *3* u = 2.68 m s^{-1}

The results of Fig. 4 are consistent with the expected behaviour of the Kenics static mixer. Relatively higher improvement of the steady-state permeate flux was observed at a modest Reynolds number in the range from 2 500 to 10 000. This can be explained by the swirling flow generated by the mixer which improved the degree of scouring of the membrane surface. However, at lower Reynolds number, the level of the swirling flow in the KM mode is insufficient to alter convection at the membrane surface to an appreciable degree. According to this hypothesis, a major reduction in the boundary layer resistance will be higher in the presence of the RI (r = 2.5 mm) mode.

Effect of Shear Rate on Flux

A more extensive study of the effect of shear rate on permeate flux was made in studies comparing the steady-state flux of ET and RI modes. (Unfortunately, the shear rate on the inner surface of membrane is difficult to approximate for the KM mode.) To facilitate the comparison between the two different modes considered, the shear rate at the inner membrane surface, assuming Newtonian fluid behaviour of the oil emulsion, was approximated for the ET mode by Eq. (*3*)

$$\gamma = 4u/R \tag{3}$$

and for RI mode by relation[14]

$$\gamma = (4\dot{V}/\pi R^3)[1 - (1 - k^2)/(2 \ln (k^{-1}))][(1 - k^4) - (1 - k^2)^2/\ln (k^{-1})]^{-1} \tag{4}$$

substituting the corresponding experimental values of superficial velocity u and volumetric flow rate $\dot{V}$, respectively.

In general, whenever an insert is placed inside the flow field, it increases the average flow velocity and the wall shear rate near the membrane surface. Also, for certain

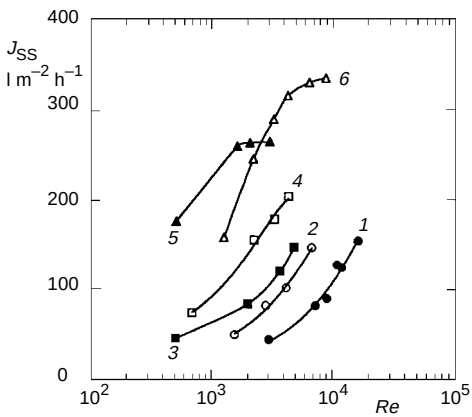

FIG. 4
Effect of Reynolds number on steady-state flux for ET, RI, and KM modes (ΔP = 200 kPa): *1* ET; *2* RI (r = 1 mm, D_e = 4 mm); *3* RI (r = 1.5 mm, D_e = 3 mm); *4* RI (r = 2 mm, D_e = 2 mm); *5* RI (r = 2.5 mm, D_e = 1 mm); *6* KM (D_e = 2.99 mm)

geometries, if the inlet flow is sufficiently high, the secondary flow or instabilities are produced which further enhance the mixing and migration of particles from the membrane surface[6,10].

As shown in Fig. 5, the steady-state permeate flux data can be correlated with the wall shear rates for both configurations examined (*i.e.*, ET and RI modes). The slope of the J_{SS}–γ plot in a log–log scale for shear rate in the range from 500 to 35 000 s^{-1} is 0.55. This value is higher than the value of one-third predicted by the concentration–polarisation model with Brownian diffusion. Another possible explanation of our results is analysis of the shear-induced diffusion model[15] in which the Brownian diffusivity is replaced by the shear-induced hydrodynamic diffusivity. The shear-induced hydrodynamic diffusivity is proportional to square of the particle size multiplied by the shear rate, whereas the Brownian diffusivity is independent of shear rate and inversely proportional to particle size. As a result, the model based on the primary mechanism of shear-induced diffusion predicts the slope of the J_{SS}–γ plot in a log–log scale close to unity[2]. Therefore, according to our results, the multiple mechanisms for particle back-diffusion or migration away from the membrane come into play[12].

Hydraulic Dissipated Power Density

The presence of inserts in the membrane tube leads to a higher resistance to the feed flow and, apparently, to higher energy consumption. To demonstrate the advantages of the use of RI inserts, the variation of the hydraulic dissipated power density with the steady-state permeate flux is shown in Fig. 6. The hydraulic dissipated power density was approximated for the ET, RI and KM modes by Eq. (*5*)

$$E_p = \Delta P_z \dot{V}/A\, J \ , \qquad (5)$$

where ΔP_z is pressure drop along the membrane tube.

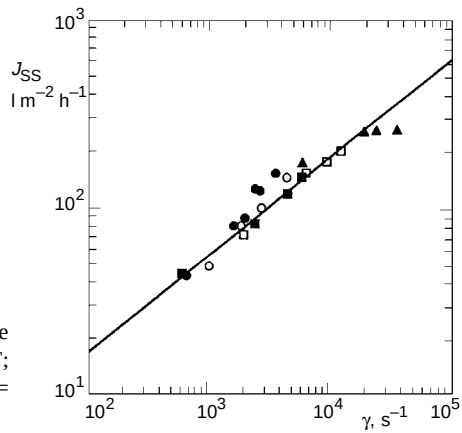

FIG. 5
Effect of wall shear rate on steady-state permeate flux for ET and RI modes (ΔP = 200 kPa): ● ET; ❍ RI (r = 1 mm); ■ RI (r = 1.5 mm); ❒ RI (r = 2 mm); ▲ RI (r = 2.5 mm)

It is obvious from Fig. 6 that the hydraulic dissipated power density gradually increases with an increase in the permeate flux, and, at a certain critical value of the permeate flux, the hydraulic dissipated power density increases sharply. Such a critical value of the permeate flux for the ET mode is lower than that for RI and KM modes. A comparison of steady-state permeate flux values shows that the RI (r = 2.5 mm) mode flux was 70% higher than the ET mode flux at the same value of the hydraulic dissipated power for both the modes. It seems that a gap of 0.5 mm between the membrane inner surface and the insert outer diameter is appropriate for a good filtration performance using this type of insert.

It follows from Fig. 6, that the steady-state permeate flux in the ET, RI (r = 1 mm) and RI (r = 1.5 mm) modes was approximately the same for the value of the hydraulic dissipated power density close to 0.5 MJ m^{-3}. On the other hand, the value of the steady-state permeate flux (approximately 200 l m^{-2} h^{-1}) was obtained in the KM mode using hydraulic dissipated power density twice higher than that observed in the RI (r = 2.5 mm) mode. Therefore this rod-shaped insert is preferred to the Kenics static mixer for the steady-state permeate flux up to 250 l m^{-2} h^{-1}.

CONCLUSIONS

The introduction of inserts, irrespective of their configuration, resulted in a significant increase of permeate flux when compared with results obtained in the empty tube system. The interruption of the formation of a boundary layer by the inserts is attributed to the mixing and migration of the rejected particles from the membrane surface. The rod-shaped inserts show (on the basis of the permeate flux and the hydraulic dissipated power density) better performance than the Kenics static mixer.

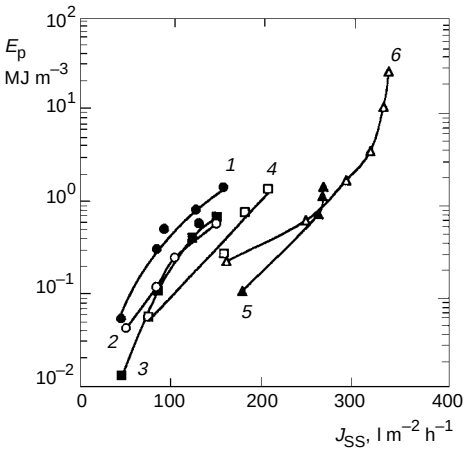

FIG. 6
Variation of hydraulic dissipated power density with steady-state permeate flux for ET, RI, and KM modes (ΔP = 200 kPa): *1* ET; *2* RI (r = 1 mm); *3* RI (r = 1.5 mm); *4* RI (r = 2 mm); *5* RI (r = 2.5 mm); *6* KM

SYMBOLS

A	inner membrane area, m^2
d	diameter of the pore or oil drop, m
D_e	equivalent hydraulic diameter, Eq. (*2*), m
E_p	hydraulic dissipated power density, Eq. (*5*), J m^{-3}
f	frequency, %
J	permeate flux, l m^{-2} h^{-1}
J_{SS}	steady-state permeate flux, l m^{-2} h^{-1}
$k = r/R$	dimensionless geometric parameter, Eq. (*4*)
o	wetted perimeter of the channel, Eq. (*2*), m
ΔP	transmembrane pressure, Pa
ΔP_z	pressure drop along the membrane tube, Pa
r	outer radius of rod insert, m
R	inner radius of membrane, m
Re	Reynolds number, Eq. (*1*)
S	cross-sectional area available for flow, Eq. (*2*), m^2
u	superficial velocity of feed, m s^{-1}
$\dot{V}$	volumetric flow rate of feed, m^3 s^{-1}
γ	shear rate at wall, Eqs (*3*) and (*4*), s^{-1}
μ	dynamic viscosity of liquid, Pa s
ρ	density of liquid, kg m^{-3}

REFERENCES

1. Mikulasek P.: Collect. Czech. Chem. Commun. *59*, 737 (1994).
2. Belfort G., Davis R. H., Zydney A. L.: J. Membr. Sci. *96*, 1 (1994).
3. Peri C., Dunkley W. L.: J. Food Sci. *36*, 395 (1971).
4. Poyen S., Quemeneur F., Bariou B.: Int. Chem. Eng. *27*, 441 (1987).
5. Thomas D. G.: Ind. Eng. Chem. Process Des. Dev. *6*, 385 (1967).
6. Finningham S. M., Howell J. A.: Chem. Eng. Res. Des. *67*, 278 (1989).
7. Pitera E. W., Middleman S.: Ind. Eng. Chem. Process Des. Dev. *12*, 52 (1973).
8. Vatai G. N., Tekic M. N.: Chem. Eng. Commun. *132*, 141 (1995).
9. Mavrov V., Nikolov N. D., Islam M. A., Nikolova J. D.: J. Membr. Sci. *75*, 197 (1992).
10. Gupta B. B., Howell J. A., Wu D., Field R. W.: J. Membr. Sci. *99*, 31 (1995).
11. Mikulasek P., Dolecek P.: Sep. Sci. Technol. *29*, 1183 (1994).
12. Ho W. S. W., Sirkar K. K.: *Membrane Handbook*. Van Nostrand Reinhold, New York 1992.
13. Belfort G.: J. Membr. Sci. *35*, 245 (1988).
14. Mikulasek P., Cakl J., Petras Z.: Presented at *3rd Int. Symp. "Progress in Membrane Science and Technology", Euromembrane '97, University of Twente.* European Society for Membrane Science and Technology, Enschede 1997.
15. Zydney A. L., Colton C. K.: Chem. Eng. Commun. *47*, 1 (1986).